High-spin states in ^{121,122}Te: Identification of favored noncollective oblate states

E. S. Paul,[1] D. B. Fossan,[2] G. J. Lane,[2] J. M. Sears,[2] I. Thorslund,[2] and P. Vaska[2]
[1]*Oliver Lodge Laboratory, University of Liverpool, PO Box 147, Liverpool L69 3BX, United Kingdom*
[2]*Department of Physics, State University of New York at Stony Brook, New York 11794*
(Received 16 November 1995)

High-spin states up to $I\sim 20\hbar$ have been studied in the ^{121,122}Te nuclei using the ^{116}Cd(^{9}Be,xn) reaction at 37.8 MeV. In this spin regime, several favored noncollective oblate states ($\gamma=+60°$), where the single-particle angular momenta generate the total nuclear spin, are predicted to coexist with weakly deformed collective structures. Theoretical expectations for such oblate states, based on TRS cranking calculations, are compared to the experimental results.

PACS number(s): 21.10.Re, 21.10.Pc, 23.20.Lv, 27.60.+j

I. INTRODUCTION

The degrees of freedom available for nuclei near closed shells are severely limited to the single-particle motion of valence nucleons. Indeed, the even tellurium ($Z=52$) isotopes, two protons beyond the $Z=50$ shell gap, show vibrational-like characteristics at low spin (e.g., Ref. [1]). The small yet finite number of valence particles is, however, able to break the spherical symmetry and induce, albeit small, nuclear deformation. The small deformation does require high angular velocity to generate collective angular momentum and hence specific noncollective ''aligned'' oblate states ($\gamma=+60°$, Lund convention [2]), where the nuclear spin is generated completely from single-particle angular-momentum contributions, are able to compete energetically with the weakly deformed collective structures. Recent investigations of light tellurium isotopes with $A\leqslant 120$ have identified several particularly low-lying states, with $I^{\pi}=14^{-}$, 16^{+}, 19^{-}, and 22^{-} in the even-A isotopes [3–7] and $I^{\pi}=21/2^{-}$, $23/2^{-}$, and $39/2^{-}$ in the odd-A isotopes [8–11]. Cranking calculations, based on the total routhian surface (TRS) formalism [12–14], suggest that these energetically favored states represent aligned noncollective oblate configurations [15].

Despite the weakly deformed low-spin structures, well-deformed ($\beta_2=0.30$–0.35) rotational ''intruder'' bands have recently been established in light Te isotopes at high spin (up to $50\hbar$) in ^{112}Te [3], ^{114}Te [16], ^{115}Te [17], and ^{116}Te [18]. These bands are believed to be based on 4-particle–2-hole proton configurations, e.g., $\pi[(h_{11/2})^2(g_{7/2})^2(g_{9/2})^{-2}]$, where two $g_{9/2}$ protons are promoted across the $Z=50$ shell gap. Similar deformed particle-hole excitations form the basis of high-spin rotational structures in Sn ($Z=50$) and Sb ($Z=51$) nuclei, e.g., Refs. 19 and 20. At the highest spins, these bands show the unique features of smooth band termination, where the nuclear shape slowly evolves from collective prolate to noncollective oblate over many transitions [21,22]. This behavior is to be contrasted to the ''abrupt'' observation of specific low-spin oblate states.

New results for ^{121,122}Te are presented in this paper, which greatly augment the known decay schemes. Since these nuclei are near the valley of stability (^{122}Te is in fact stable), they are difficult to populate using heavy-ion fusion-evaporation reactions that could bring in sufficient angular momentum to study the high-spin collective features. Therefore the present results, using a ^{9}Be beam and ^{116}Cd target, focus on the low-spin structures with $I\leqslant 20\hbar$, where however specific low-lying (yrast) noncollective oblate states are expected to be observed. Previous work on ^{121}Te has been published in Ref. [23] using the ^{119}Sn($\alpha,2n\gamma$) reaction, and very recently in Ref. [10] using the ^{110}Pd(^{18}O,$\alpha 3n\gamma$) reaction, and Ref. [11] using the ^{114}Cd(^{11}B,$p3n\gamma$) reaction; previous data on ^{122}Te, obtained with the ^{120}Sn($\alpha,2n\gamma$) reaction, can be found in Ref. [24].

II. EXPERIMENTAL METHODS AND RESULTS

Following an excitation-function measurement, high-spin states in ^{121,122}Te were populated with the ^{116}Cd(^{9}Be, xn)$^{125-x}$Te reaction at a bombarding energy of 37.8 MeV. At this beam energy, states in ^{121}Te and ^{122}Te were populated with approximately equal strength. The ^{9}Be beam, provided by the Stony Brook Tandem/Linac accelerator, was incident upon a ^{116}Cd target of thickness 3.2 mg/cm^2 mounted on a thick lead backing, which served to stop the recoiling nuclei prior to γ-ray emission. Coincident γ-γ data were acquired with an array of six Compton-suppressed HPGe detectors (each 25% efficient), plus a 14-element bismuth germanate (BGO) multiplicity/sum-energy filter. In order to suppress low-multiplicity γ-ray events from Coulomb excitation and radioactive decay, data were written onto magnetic tape only for events in which two or more suppressed HPGe detectors registered in prompt time coincidence ($\tau\leqslant 100$ ns) with one or more BGO elements. The use of a backed target maintained excellent energy resolution; $\Delta E_{\gamma}=2.4$ keV was achieved at $E_{\gamma}=1$ MeV. Careful energy calibrations were performed both before and after this 4-day experiment using a ^{152}Eu radioactive source and no gain shifts were observed during the experiment. The γ-ray data were gain-matched before being written to tape and approximately 37 million γ-γ events were recorded. Efficiency calibrations of the detectors were achieved using ^{152}Eu and ^{133}Ba radioactive sources.

The coincidence analysis of the data and level scheme construction were greatly facilitated by the use of the ESCL8R graphical analysis package [25]. In addition, angular-correlation information was obtained from the coin-

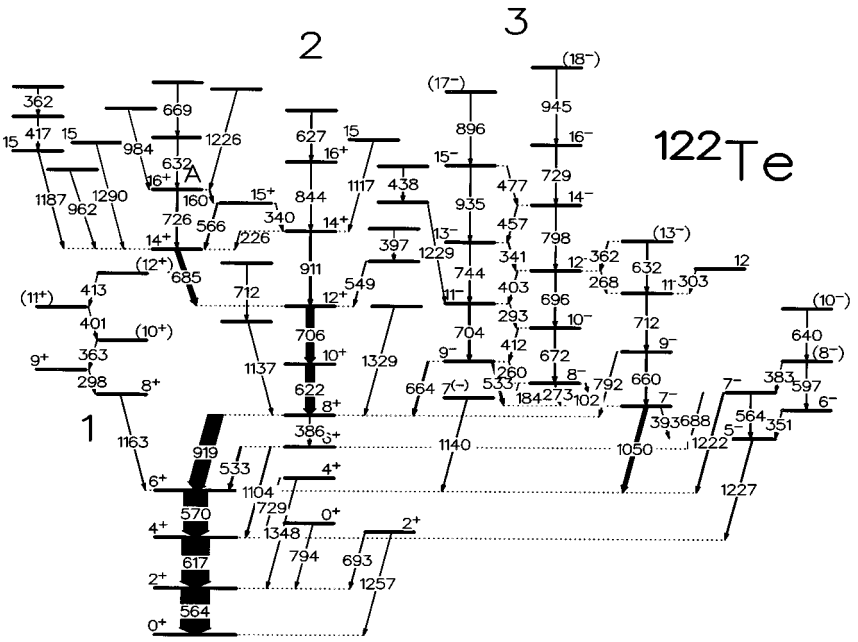

FIG. 1. Level scheme deduced for ^{122}Te. The transition energies are given in keV and their relative intensities are proportional to the widths of the arrows.

cidence data by sorting a matrix of the four forward/backward detectors ($\theta \sim 35°/145°$) against the two detectors near $\theta = 90°$. Angular intensity ratios,

$$R_{\mathrm{DCO}} = \frac{I_\gamma(35° - 90°)}{I_\gamma(90° - 35°)}, \tag{1}$$

of γ rays extracted from this matrix were used to assist in the assignment of transition multipolarities using the method of directional correlation from oriented states (DCO) [26]. For the present geometry, values of $R_{\mathrm{DCO}} \approx 1.00$ are expected for stretched quadrupole transitions, while values of $R_{\mathrm{DCO}} \approx 0.55$ are expected for pure stretched dipole transitions, when gating on stretched $E2$ transitions. The decay schemes of ^{121,122}Te deduced from this work, together with representative gated γ-ray spectra, are shown in Figs. 1–4. Transition energies, relative intensities, DCO results, and assignments are listed in Tables I and II. Where possible, transition intensities have been used to extract experimental $B(M1; I \to I-1)/B(E2; I \to I-2)$ ratios of reduced transition probabilities and the results are presented in Fig. 5.

A. The level scheme of ^{122}Te

The level scheme deduced for ^{122}Te is shown in Fig. 1, while Table I lists the γ-ray properties. Examples of gated coincidence spectra are shown in Fig. 2. The ordering of the transitions in the level scheme is based on relative intensities and coincidence relationships. Many new states have been established, including states above the 12^+ state [24] of band 2, together with the negative-parity sequences shown to the right and band 1 shown to the left. Two states have been established at $I^\pi = 14^+$ and two at 16^+. Several high-energy transitions feed the yrast 14^+ and 16^+ states. The spins and parities of the negative-parity bands are established through the DCO ratios of the linking 664, 1140, 1050, 1222, and 1227 keV transitions which suggest pure dipole ($E1$) character. These assignments are consistent with previous work [24].

B. The level scheme of ^{121}Te

The level scheme deduced for ^{121}Te is shown in Fig. 3; the transitions that feed the low-spin negative-parity states are shown in Fig. 3(a), while the positive-parity states are shown in Fig. 3(b). Table II lists the energies, intensities, and angular-correlation information for the transitions, and examples of gated coincidence spectra are shown in Fig. 4. Again, the ordering of the transitions in the level scheme is based on relative intensities and coincidence relationships.

The $11/2^-$ state in Fig. 3(a) lies 293 keV above the $1/2^+$ ground state and is isomeric with a half-life $t_{1/2} = 154$ days [23]. The $7/2^+$ state of band 6 in Fig. 3(b) is also

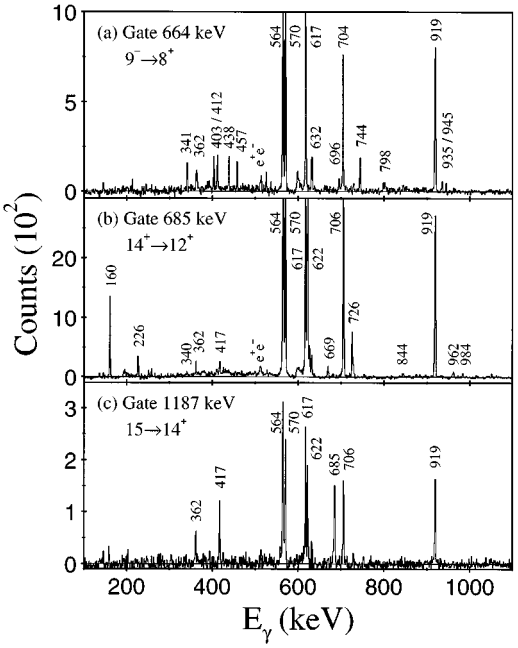

FIG. 2. Examples of gated coincidence spectra showing transitions in ^{122}Te.

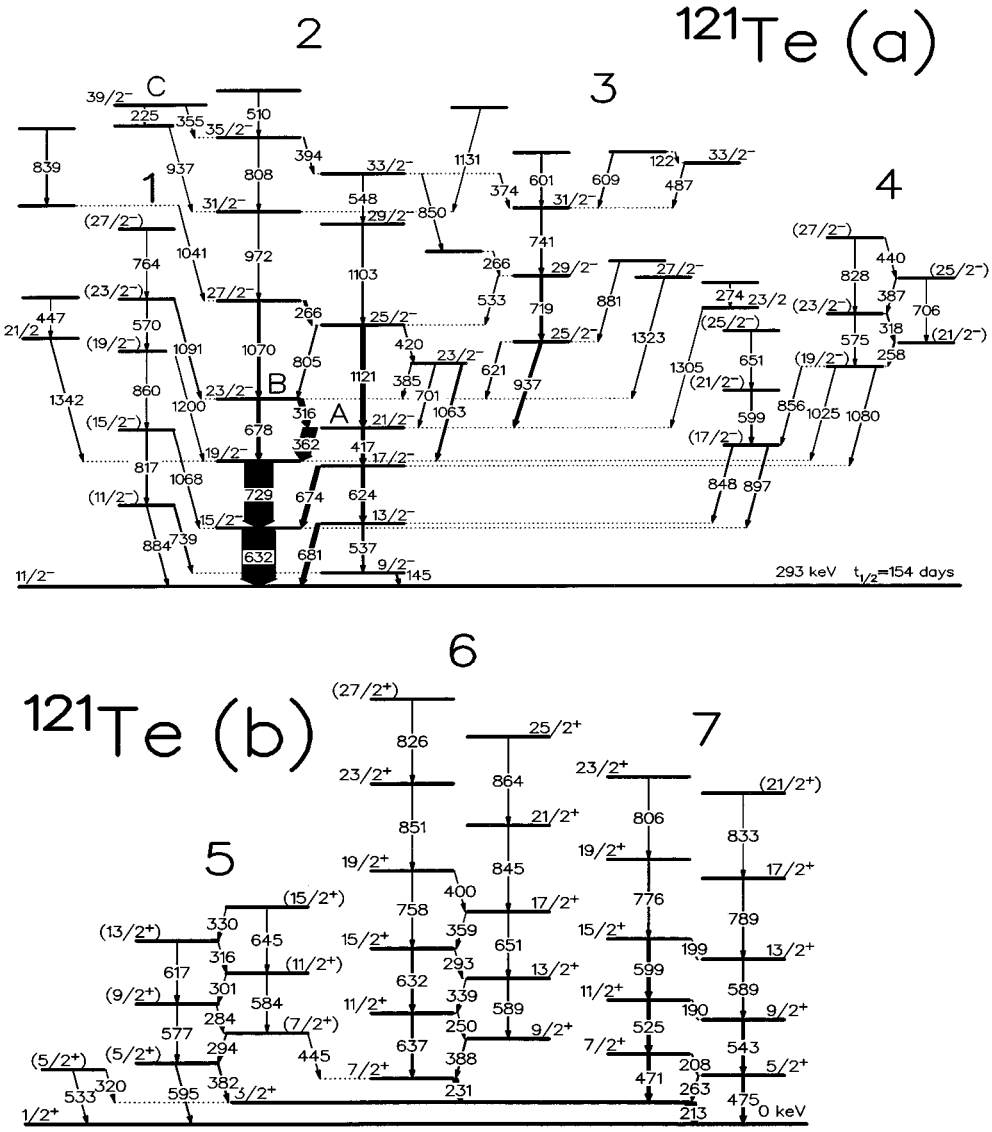

FIG. 3. Level scheme deduced for ^{121}Te. The transition energies are given in keV and their relative intensities are proportional to the widths of the arrows.

isomeric with a half-life $t_{1/2}=86$ ns [23]. The negative-parity levels shown in Fig. 3(a) (band 2) corroborate the recent work of Refs. 10 and 11, where higher spins than the present work were obtained. Many new states are shown in Fig. 3(a); bands 1 and 4 have been established for the first time. In Fig. 3(b), band 5 has been extended above the $(9/2^+)$ state, band 6 above the $17/2^+$ state, and band 7 above the $15/2^+$ state [23]. Despite the low DCO ratio obtained from the present experiment for the 231 keV transition, which depopulates band 6, an $E2$ assignment is adopted from Ref. [23], where γ-ray angular distribution and linear polarisation measurements were performed. The 231 keV transition decays from an 86 ns isomer [23], which may explain the low DCO value obtained in the present work.

III. DISCUSSION

A. Positive-parity states in ^{122}Te

As in other even-A Te isotopes, the ground-state band in ^{122}Te appears vibrational rather than rotational, see Ref. [1]. For example, the $E(4^+)/E(2^+)$ energy ratio in ^{122}Te is 2.09 which is much closer to the pure vibrational limit (2.00) than to the rotational limit (3.33). The 2^+-8^+ sequence may represent 1–4-phonon vibrational states. The 6^+ state, which is seen at a very similar excitation energy in the isotopes with $A\geqslant 116$, has also been interpreted in terms of a 2-quasiproton state where $\pi[(g_{7/2})^2]_{6^+}$ or $\pi[g_{7/2}d_{5/2}]_{6^+}$ proton configurations are coupled to the spherical Sn ($Z=50$) core states [1,7].

At spin 10^+ and above, the positive-parity states may be interpreted in terms of an aligned 2-quasineutron $\nu[(h_{11/2})^2]$ configuration which is expected at a lower excitation energy than the 5-phonon 10^+ state. Above the 12^+ state of band 2, the level structure becomes rather complex. Two 14^+ and two 16^+ states are evident in Fig. 1. The yrast 16^+ state, labeled A, decays to the yrast 14^+ state via the 726 keV transition, in addition to decaying into the second 14^+ state via an intermediate 15^+ state.

The short cascade of four dipole transitions, shown to the left in Fig. 1 (band 1), suggests the involvement of a $g_{9/2}^{-1}$ orbital, i.e., a 3-particle–1-hole proton structure relative to the magic $Z=50$ core. Similar excitations involving a single $g_{9/2}^{-1}$ orbital give rise to collective $\Delta I=1$ dipole bands in Sn

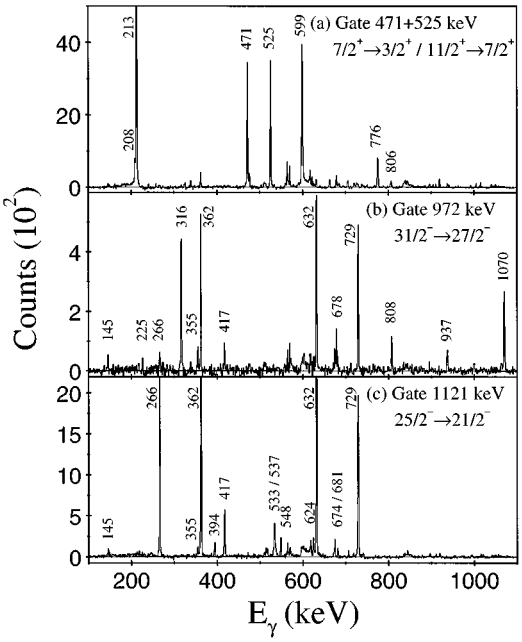

FIG. 4. Examples of gated coincidence spectra showing transitions in ^{121}Te.

($Z=50$), Sb ($Z=51$), and I ($Z=53$) nuclei [27]. The $I^{\pi}=8^{+}$ band-head suggests a $\pi[(g_{9/2})^{-1}g_{7/2}]_{8^+}\otimes[(d_{5/2})^2]_{0^+}$ proton structure for band 1 in ^{122}Te.

B. Negative-parity states in ^{122}Te

Negative-parity 2-quasineutron states may be formed in ^{122}Te by coupling a high-j $\nu h_{11/2}$ orbital to the available $\nu g_{7/2}$, $\nu d_{5/2}$, and $\nu d_{3/2}$ orbitals that are near the $N=70$ Fermi surface for prolate deformation. These three positive-parity neutron orbitals are seen in ^{121}Te, as discussed in Sec. III D. The relatively small signature splitting at low spin for band 3 in Fig. 1, with the odd spins favored, is consistent with a ν $[h_{11/2}g_{7/2}]$ structure; this structure has the favored signature $\alpha=1$ ($I=\alpha \bmod 2$). The $B(M1;I\rightarrow I-1)/B(E2;I\rightarrow I-2)$ ratios extracted for band 3, shown in Fig. 5, increase significantly with increasing spin and may indicate a loss of collectivity.

C. Negative-parity states in ^{121}Te

Negative-parity bands in odd-A Te isotopes are associated with a $\nu h_{11/2}$ orbital. As in the neighboring odd-A isotopes, both signatures of this orbital are seen in ^{121}Te, labeled as band 2 in Fig. 3(a). The states at $I^{\pi}=21/2^{-}$ [labeled A in Fig. 3(a)] and $23/3^{-}$ (labeled B) are unusually low-lying and a sharp increase in the $B(M1;I\rightarrow I-1)/B(E2;I\rightarrow I-2)$ ratios occurs at this point, as shown in Fig. 5. High-energy γ rays continue both signatures of the band above these states until a low-lying $39/2^{-}$ state (labeled C) is observed after the low-energy 355 keV quadrupole transition. A parallel decay branch of 255 keV and 937 keV transitions also depopulate this state. The nature of these low-lying states will be discussed in regard to TRS cranking calculations in Sec. III E.

Band 1 consists of a series of states with signature $\alpha=-1/2$ and could represent the favored signature of the

TABLE I. Properties of the transitions assigned to ^{122}Te.

E_γ (keV)[a]	I_γ[b]	R_{DCO}[c]	Multipolarity	Assignment
102.5	1.26	0.43(1)	$M1/E2$	$8^-\rightarrow 7^-$
160.5	2.34	0.42(1)	$M1/E2$	$16^+\rightarrow 15^+$
183.8	0.32		$(M1/E2)$	$8^-\rightarrow 7^{(-)}$
225.8	0.65	0.62(2)	$M1/E2$	$14^+\rightarrow 14^+$
260.1	0.63	0.95(3)	$M1/E2$	$9^-\rightarrow 8^-$
268.3	0.34		$(M1/E2)$	$12^-\rightarrow 11^-$
273.4	3.30	1.00(2)	$M1/E2$	$8^-\rightarrow 7^-$
292.8	0.47		$(M1/E2)$	$11^-\rightarrow 10^-$
297.6	0.73	0.66(2)	$(M1/E2)$	$9^+\rightarrow 8^+$
303.3	0.66	0.47(2)	dipole	$12\rightarrow 11^-$
340.5	0.76	0.38(1)	$M1/E2$	$15^+\rightarrow 14^+$
340.6	1.90		$(M1/E2)$	$13^-\rightarrow 12^-$
351.5	1.26	0.55(2)	$M1/E2$	$6^-\rightarrow 5^-$
361.7	0.58			
362.5	2.19		$(M1/E2)$	$(13^-)\rightarrow 12^-$
363.1	0.52		$(M1/E2)$	$(10^+)\rightarrow 9^+$
383.4	0.40		$(M1/E2)$	$(8^-)\rightarrow 7^-$
386.0	1.28		$(E2)$	$8^+\rightarrow 6^+$
393.2	0.80		$E2$	$7^-\rightarrow 5^-$
397.1	0.76			
400.9	0.26		$(M1/E2)$	$(11^+\rightarrow 10^+)$
403.1	1.89		$(M1/E2)$	$12^-\rightarrow 11^-$
411.7	1.95		$(M1/E2)$	$10^-\rightarrow 9^-$
413.1	0.12		$(M1/E2)$	$(12^+\rightarrow 11^+)$
417.0	1.01			$\rightarrow 15^+$
437.8	0.60			
457.2	1.58	0.25(2)	$M1/E2$	$14^-\rightarrow 13^-$
476.6	0.60		$(M1/E2)$	$15^-\rightarrow 14^-$
532.9	6.15	0.78(2)[d]	$(E2)$	$9^-\rightarrow 7^-$
533.0	5.5	0.78(2)[d]	$(M1/E2)$	$6^+\rightarrow 6^+$
548.7	2.16			$\rightarrow 12^+$
564.1	115	0.97(1)	$E2$	$2^+\rightarrow 0^+$
564.2	3.39		$(E2)$	$7^-\rightarrow 5^-$
566.1	3.59		$(M1/E2)$	$15^+\rightarrow 14^+$
570.0	95.3	1.03(1)	$E2$	$6^+\rightarrow 4^+$
597.0	1.39		$(E2)$	$(8^-)\rightarrow 6^-$
617.3	109	1.05(1)	$E2$	$4^+\rightarrow 2^+$
622.1	34.8	1.08(1)	$E2$	$10^+\rightarrow 8^+$
626.6	2.16			$\rightarrow 16^+$
631.6	2.83		$(E2)$	$(13^-)\rightarrow 11^-$
631.7	1.15			$\rightarrow 16^+$
639.6	0.69		$(E2)$	$(10^-\rightarrow 8^-)$
664.1	5.31	0.48(1)	$E1$	$9^-\rightarrow 8^+$
660.5	4.39	0.92(2)	$E2$	$9^-\rightarrow 7^-$
669.3	1.04			
671.6	5.22	1.10(3)	$E2$	$10^-\rightarrow 8^-$
685.0	17.7	1.08(2)	$E2$	$14^+\rightarrow 12^+$
688.1	2.27		$(E1)$	$7^-\rightarrow 6^+$
693.3	1.73		$(M1/E2)$	$2^+\rightarrow 2^{+\,e}$
695.8	3.53	0.97(2)	$E2$	$12^-\rightarrow 10^-$
704.4	6.74	1.04(2)[f]	$E2$	$11^-\rightarrow 9^-$
705.6	29.7	1.04(2)[f]	$E2$	$12^+\rightarrow 10^+$
712.2	4.51	0.92(2)[g]	$E2$	$11^-\rightarrow 9^-$
712.4	0.75	0.92(2)[g]		
726.0	3.17		$(E2)$	$16^+\rightarrow 14^+$

TABLE I. (*Continued*).

E_γ (keV)[a]	I_γ[b]	R_{DCO}[c]	Multipolarity	Assignment
728.6	1.36		$(M1/E2)$	$4^+ \rightarrow 4^+$ [e]
729.2	1.93	1.12(3)	$E2$	$16^- \rightarrow 14^-$
743.8	2.93	1.07(3)	$E2$	$13^- \rightarrow 11^-$
791.7	2.04	0.52(2)	$E1$	$9^- \rightarrow 8^+$
793.6	0.88		$(E2)$	$0^+ \rightarrow 2^+$ [e]
798.1	1.08	0.93(5)	$E2$	$14^- \rightarrow 12^-$
844.1	2.21	1.14(4)	$E2$	$16^+ \rightarrow 14^+$
896.2	1.00		$(E2)$	$(17^-) \rightarrow 15^-$
910.6	5.88	0.98(2)	$E2$	$14^+ \rightarrow 12^+$
919.0	60.5	1.06(1)	$E2$	$8^+ \rightarrow 6^+$
935.1	1.34	1.20(6)	$E2$	$15^- \rightarrow 13^-$
945.0	0.75		$(E2)$	$(18^-) \rightarrow 16^-$
961.7	0.81			$\rightarrow 14^+$
983.6	0.39			$\rightarrow 16^+$
1050.0	15.2	0.58(1)	$E1$	$7^- \rightarrow 6^+$
1103.4	3.48	1.15(5)	$E2$	$6^+ \rightarrow 4^+$
1117.0	0.91	0.71(2)	dipole	$15 \rightarrow 14^+$
1136.4	0.73			$\rightarrow 8^+$
1140.1	2.12	0.43(2)	$(E1)$	$7^{(-)} \rightarrow 6^+$
1163.0	1.54	1.02(3)	$E2$	$8^+ \rightarrow 6^+$
1186.7	1.16	0.57(2)	dipole	$15 \rightarrow 14^+$
1221.6	4.44	0.59(2)	$E1$	$7^- \rightarrow 6^+$
1225.8	0.78			$\rightarrow 16^+$
1227.3	3.50	0.65(3)	$E1$	$5^- \rightarrow 4^+$
1229.2	0.55			$\rightarrow 11^-$
1256.9	0.90		$(E2)$	$2^+ \rightarrow 0^+$ [e]
1290.3	0.56	0.74(3)	dipole	$15 \rightarrow 14^+$
1329.1	1.15			$\rightarrow 8^+$
1346.5	1.52		$(E2)$	$4^+ \rightarrow 2^+$ [e]

[a]Energies are accurate to ± 0.2 keV. A linear energy calibration has been used.
[b]Relative intensities are accurate to $\pm 10\%$.
[c]The ratios were obtained from summed spectra gated by the 564.1, 617.3, 570.0, 919.0, and 622.1 keV $E2$ transitions.
[d]Doublet, value given for the 532.9–533.0 keV summed peak.
[e]Assignment taken from Ref. [24].
[f]Doublet, value given for the 704.4–705.6 keV summed peak.
[g]Doublet, value given for the 712.2–712.4 keV summed peak.

second available $\nu h_{11/2}$ orbital. Alternatively, this structure may represent the first $\nu h_{11/2}$ orbital coupled to the γ-vibrational band of the core. Such structures have been proposed for similar bands in odd-A I ($Z=53$) [28] and Cs ($Z=55$) [29] isotopes. As in band 2, the $23/2^-$ state of band 1 is unusually low lying. Band 3 consists of yrast $25/2^-$ and $29/2^-$ states and possibly represents a 3-quasineutron structure.

Band 4 has large $B(M1;I \rightarrow I-1)/B(E2;I \rightarrow I-2)$ ratios (see Fig. 5), and is most likely built on a 3-quasiparticle configuration. The high ratios suggest involvement of a 3-particle–1-hole proton structure, including a single $g_{9/2}^{-1}$ orbital, coupled to the odd neutron. A possible structure is formed by the coupling of a $\nu h_{11/2}$ orbital to the proton structure proposed for band 1 in ^{122}Te, namely, the $\pi[(g_{9/2})^{-1} g_{7/2}]_{8^+} \otimes [(d_{5/2})^2]_{0^+}$ configuration.

TABLE II. Properties of the transitions assigned to ^{121}Te.

E_γ (keV)[a]	I_γ[b]	R_{DCO}[c]	Multipolarity	Assignment
122.4	0.14			$\rightarrow 33/2^-$
145.1	3.51	0.58(2)[d]	$M1/E2$	$9/2^- \rightarrow 11/2^-$
189.9	0.43	0.60(4)[e]	$M1/E2$	$11/2^+ \rightarrow 9/2^+$
199.4	0.14		$(M1/E2)$	$15/2^+ \rightarrow 13/2^+$
208.2	1.70	0.72(3)	$M1/E2$	$7/2^+ \rightarrow 5/2^+$
212.6	32.8	0.63(1)[f]	$M1/E2$	$3/2^+ \rightarrow 1/2^+$
225.2	0.12			$39/2^- \rightarrow$
231.3	15.6	0.68(2)[g]	$E2$[h]	$7/2^+ \rightarrow 3/2^+$
249.9	0.14		$(M1/E2)$	$11/2^+ \rightarrow 9/2^+$
257.7	3.16	0.60(3)	$M1/E2$	$(21/2^- \rightarrow 19/2^-)$
263.5	2.15	0.75(4)	$M1/E2$	$5/2^+ \rightarrow 3/2^+$
265.7	0.40			$\rightarrow 29/2^-$
265.8	8.22	0.43(3)	$M1/E2$	$27/2^- \rightarrow 25/2^-$
273.8	0.18			$\rightarrow 23/2$
283.8	0.49		$(M1/E2)$	$(9/2^+ \rightarrow 7/2^+)$
292.8	0.37	0.39(3)[i]	$M1/E2$	$15/2^+ \rightarrow 13/2^+$
293.6	1.52		$(M1/E2)$	$(7/2^+ \rightarrow 5/2^+)$
300.9	0.28		$(M1/E2)$	$(11/2^+ \rightarrow 9/2^+)$
316.0	0.36		$(M1/E2)$	$(13/2^+ \rightarrow 11/2^+)$
316.4	19.8	0.43(1)	$M1/E2$	$23/2^- \rightarrow 21/2^-$
318.1	2.31		$(M1/E2)$	$(23/2^- \rightarrow 21/2^-)$
319.9	0.29		$(M1/E2)$	$(5/2^+) \rightarrow 3/2^+$
330.4	0.10		$(M1/E2)$	$(15/2^+ \rightarrow 13/2^+)$
339.4	0.40	0.28(2)[g]	$M1/E2$	$13/2^+ \rightarrow 11/2^+$
354.6	1.06	0.89(5)	$E2$[j]	$39/2^- \rightarrow 35/2^-$
358.7	0.36	0.39(4)[g]	$M1/E2$	$17/2^+ \rightarrow 15/2^+$
361.9	49.2	0.33(1)	$M1/E2$	$21/2^- \rightarrow 19/2^-$
374.1	0.71		$(M1/E2)$	$33/2^- \rightarrow 31/2^-$
382.5	2.92		$(M1/E2)$	$(5/2^+) \rightarrow 3/2^+$
384.8	1.48	0.74(4)	$M1/E2$	$23/2^- \rightarrow 23/2^-$
387.5	1.41		$(M1/E2)$	$(25/2^- \rightarrow 23/2^-)$
387.6	2.57	0.47(2)[i]	$M1/E2$	$9/2^+ \rightarrow 7/2^+$
393.9	1.34	0.43(2)	$M1/E2$	$35/2^- \rightarrow 31/2^-$
399.5	0.11		$(M1/E2)$	$19/2^+ \rightarrow 17/2^+$
416.6	10.3	1.06(5)[d]	$E2$	$21/2^- \rightarrow 17/2^-$
419.9	2.11	0.56(3)	$M1/E2$	$25/2^- \rightarrow 23/2^-$
440.4	0.67		$(M1/E2)$	$(27/2^- \rightarrow 25/2^-)$
445.0	0.12		$(M1/E2)$	$(7/2^+) \rightarrow 7/2^+$
446.6	0.39			$\rightarrow 21/2$
471.0	10.09	1.00(2)[f]	$E2$	$7/2^+ \rightarrow 3/2^+$
475.4	8.61	0.98(2)[e]	$E2$	$5/2^+ \rightarrow 1/2^+$
487.4	1.05	0.43(3)	$M1/E2$	$33/2^- \rightarrow 31/2^-$
510.5	0.76			$\rightarrow 35/2^-$
525.1	10.14	1.01(2)[f]	$E2$	$11/2^+ \rightarrow 7/2^+$
533.1	0.79		$(E2)$	$(5/2^+) \rightarrow 1/2^+$
533.3	1.16		$(E2)$	$29/2^- \rightarrow 25/2^-$
536.7	3.63	0.94(5)[d]	$E2$	$13/2^- \rightarrow 9/2^-$
543.3	5.39	1.00(2)[e]	$E2$	$9/2^+ \rightarrow 5/2^+$
547.6	1.87	1.11(8)[d]	$E2$	$33/2^- \rightarrow 29/2^-$
570.1	1.49		$(E2)$	$(23/2^- \rightarrow 19/2^-)$
575.4	0.28		$(E2)$	$(23/2^- \rightarrow 19/2^-)$
577.0	1.09		$(E2)$	$(9/2^+ \rightarrow 5/2^+)$
584.4	0.47		$(E2)$	$(11/2^+ \rightarrow 7/2^+)$
588.9	2.65	1.00(2)[i]	$E2$	$13/2^+ \rightarrow 9/2^+$
589.0	2.97	1.02(2)[e]	$E2$	$13/2^+ \rightarrow 9/2^+$

TABLE II. (*Continued*).

E_γ (keV)[a]	I_γ[b]	R_{DCO}[c]	Multipolarity	Assignment
595.4	1.78		$(E2)$	$(5/2^+)\rightarrow 1/2^+$
598.6	9.09	1.05(2)[f]	$E2$	$15/2^+\rightarrow 11/2^+$
598.9	3.65		$(E2)$	$(21/2^-\rightarrow 17/2^-)$
601.4	1.70			$\rightarrow 31/2^-$
609.2	2.32			$\rightarrow 31/2^-$
617.0	2.25		$(E2)$	$(13/2^+\rightarrow 9/2^+)$
621.3	2.32		$(M1/E2)$	$25/2^-\rightarrow 23/2^-$
624.5	11.5	1.03(3)[d]	$E2$	$17/2^-\rightarrow 13/2^-$
631.7	4.51	1.06(3)[g]	$E2$	$15/2^+\rightarrow 11/2^+$
631.7	118	1.00(1)	$E2$	$15/2^-\rightarrow 11/2^-$
637.4	3.79	1.10(5)[g]	$E2$	$11/2^+\rightarrow 7/2^+$
645.3	0.26		$(E2)$	$(15/2^+\rightarrow 11/2^+)$
651.0	1.74	1.02(2)[i]	$E2$	$17/2^+\rightarrow 13/2^+$
651.0	0.55		$(E2)$	$(25/2^-\rightarrow 21/2^-)$
674.1	15.3	0.20(1)	$M1/E2$	$17/2^-\rightarrow 15/2^-$
678.2	10.5	1.01(2)	$E2$	$23/2^-\rightarrow 19/2^-$
681.4	15.3	0.35(2)[d]	$M1/E2$	$13/2^-\rightarrow 11/2^-$
700.9	2.57	0.33(2)	$M1/E2$	$23/2^-\rightarrow 21/2^-$
705.7	0.55		$(E2)$	$(25/2^-\rightarrow 21/2^-)$
719.4	8.20	0.94(3)	$E2$	$29/2^-\rightarrow 25/2^-$
729.0	101	1.01(1)	$E2$	$19/2^-\rightarrow 15/2^-$
739.2	3.78		$(M1/E2)$	$(11/2^-)\rightarrow 9/2^-$
740.5	5.02	0.67(3)	$M1/E2$	$31/2^-\rightarrow 29/2^-$
757.9	1.41	0.93(4)[g]	$E2$	$19/2^+\rightarrow 15/2^+$
764.2	0.58		$(E2)$	$(27/2^-\rightarrow 23/2^-)$
775.8	2.18	0.97(4)[f]	$E2$	$19/2^+\rightarrow 15/2^+$
788.7	1.44	1.08(4)[e]	$E2$	$17/2^+\rightarrow 13/2^+$
804.7	2.70	0.34(2)	$M1/E2$	$25/2^-\rightarrow 23/2^-$
806.4	0.48	0.95(5)[f]	$E2$	$23/2^+\rightarrow 19/2^+$
807.7	0.29	1.04(5)	$E2$	$35/2^-\rightarrow 31/2^-$
817.0	2.82		$(E2)$	$(15/2^-\rightarrow 11/2^-)$
826.0	0.12		$(E2)$	$(27/2^+)\rightarrow 23/2^+$
828.2	0.20		$(E2)$	$(27/2^-\rightarrow 23/2^-)$
832.8	0.12		$(E2)$	$(21/2^+)\rightarrow 17/2^+$
838.5	1.91			
844.6	1.58	0.96(3)[i]	$E2$	$21/2^+\rightarrow 17/2^+$
848.4	2.86	0.91(5)	$(E2)$	$(17/2^-)\rightarrow 13/2^-$
849.5	0.95			$33/2^-\rightarrow$
851.0	0.74	0.94(5)[g]	$E2$	$23/2^+\rightarrow 19/2^+$
856.2	1.53		$(M1/E2)$	$(19/2^-\rightarrow 17/2^-)$
860.3	0.75		$(E2)$	$(19/2^-)\rightarrow 15/2^-$
864.2	0.27	1.02(5)[i]	$E2$	$25/2^+\rightarrow 21/2^+$
881.3	1.27			$\rightarrow 25/2^-$
883.9	2.10		$(M1/E2)$	$(11/2^-)\rightarrow 11/2^-$
897.3	3.69	0.82(5)	$(M1/E2)$	$(17/2^-)\rightarrow 15/2^-$
937.1	0.13			$\rightarrow 31/2^-$
937.4	9.50	0.94(3)	$E2$	$25/2^-\rightarrow 21/2^-$
971.9	1.65	0.97(4)	$E2$	$31/2^-\rightarrow 27/2^-$
1025.0	0.97		$(M1/E2)$	$(19/2^-)\rightarrow 19/2^-$
1040.9	0.87			$\rightarrow 27/2^-$
1063.1	6.13	0.93(4)	$E2$	$23/2^-\rightarrow 19/2^-$
1068.0	1.99	0.81(5)	$M1/E2$	$(15/2^-)\rightarrow 15/2^-$
1070.2	8.27	0.96(5)	$E2$	$27/2^-\rightarrow 23/2^-$
1079.9	1.58	0.63(5)	$(M1/E2)$	$(19/2^-)\rightarrow 17/2^-$

TABLE II. (*Continued*).

E_γ (keV)[a]	I_γ[b]	R_{DCO}[c]	Multipolarity	Assignment
1091.1	2.63	0.67(5)	$M1/E2$	$(23/2^-)\rightarrow 23/2^-$
1103.2	2.74	0.97(4)	$E2$	$29/2^-\rightarrow 25/2^-$
1121.4	13.9	1.01(4)[d]	$E2$	$25/2^-\rightarrow 21/2^-$
1131.1	0.46			$\rightarrow 31/2^-$
1200.1	0.61		$(M1/E2)$	$(19/2^-)\rightarrow 19/2^-$
1304.9	0.35	0.47(6)	dipole	$23/3\rightarrow 21/2^-$
1323.2	0.93	1.11(9)	$E2$	$27/2^-\rightarrow 23/2^-$
1342.2	1.53	0.50(6)	dipole	$21/2\rightarrow 19/2^-$

[a]Energies are accurate to ± 0.2 keV. A linear energy calibration has been used.

[b]Relative intensities are accurate to $\pm 10\%$.

[c]Except where stated, the ratios were obtained from summed spectra gated by the 631.7 and 729.0 keV $E2$ transitions.

[d]Ratio obtained from summed spectra gated by the 536.7, 416.6, and 1121.4 keV $E2$ transitions.

[e]Ratio obtained from summed spectra gated by the 475.4 and 543.3 keV $E2$ transitions.

[f]Ratio obtained from summed spectra gated by the 471.0 and 525.1 keV $E2$ transitions.

[g]Adopted from Ref. [23] where angular distribution and linear polarization measurements were performed.

[h]Ratio obtained from summed spectra gated by the 588.9 and 651.0 keV $E2$ transitions.

[i]Adopted from Ref. [10].

D. Positive-parity states in ^{121}Te

The three positive-parity band structures shown in Fig. 3(b) are interpreted in terms of weakly deformed prolate structures, based on $\nu d_{5/2}$ (band 5), $\nu g_{7/2}$ (band 6), and $\nu d_{3/2}$ (band 7) orbitals (see TRS results in the following section). Indeed, high-Ω ($\Omega = j$) $\nu g_{7/2}$ and $\nu d_{5/2}$ orbitals are near the Fermi surface for $N=69$, together with low-j $\nu d_{3/2}$ and $\nu s_{1/2}$ ($\Omega = 1/2$) orbitals. The higher $B(M1;I\rightarrow I-1)/B(E2;I\rightarrow I-2)$ ratios, shown in Fig. 5, found for band 5 as compared to band 6 are consistent with

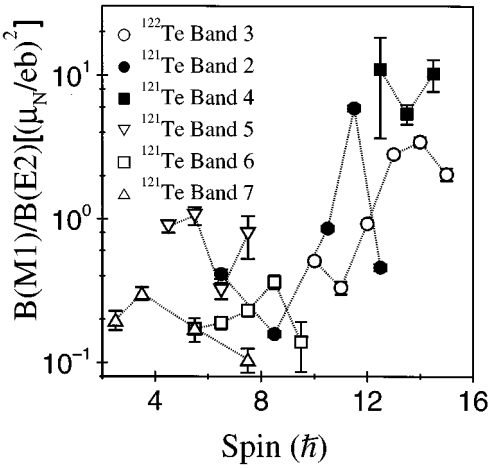

FIG. 5. Experimental $B(M1;I\rightarrow I-1)/B(E2;I\rightarrow I-2)$ ratios of reduced transition probabilities for bands in ^{122}Te and ^{121}Te.

TABLE III. TRS calculated favoured noncollective oblate ($\gamma=+60°$) states in ^{122}Te.

(Parity, signature)	I^π	β_2	Aligned configuration
(+,0)	16^+	0.115	$\pi[(g_{7/2})^2]_{6^+}\otimes\nu[(h_{11/2})^2]_{10^+}$
(+,0)	22^+	0.112	$\pi[(g_{7/2})^2]_{6^+}\otimes\nu[(h_{11/2})^4]_{16^+}$
(−,0)	22^-	0.111	$\pi[(g_{7/2})^2]_{6^+}\otimes\nu[(d_{5/2})(h_{11/2})^3]_{16^-}$

these assignments, i.e., band 5 is based on a $\nu d_{5/2}$ ($j=l+1/2$) orbital which has a larger magnetic moment than the $\nu g_{7/2}$ ($j=l-1/2$) orbital of band 6.

E. TRS calculations

Deformation self-consistent cranking calculations, based on the TRS formalism [12–14] and using a deformed Woods-Saxon single-particle potential [30,31] have been performed for quasiparticle configurations in light Te isotopes, as discussed in Ref. [15]. Generally, weakly deformed collective shapes are predicted at low spin which coexist with several specific noncollective oblate states, some of which are predicted to be yrast.

At low spin in even-A ^{122}Te, the TRS calculations suggest a weakly deformed collective oblate shape for the ground-state band with $\beta_2=0.13$, $\gamma\sim-60°$. At higher spin, the 2-quasineutron $\nu[(h_{11/2})^2]$ configuration becomes yrast with triaxial deformation parameters $\beta_2=0.16$, $\gamma\sim-45°$. Negative-parity structures, based on 2-quasineutron $\nu[h_{11/2}g_{7/2}]$ and $\nu[h_{11/2}d_{5/2}]$ configurations, are similarly triaxial with $\beta_2=0.14$, $\gamma\sim-45°$.

At low spin in odd-A ^{121}Te, negative-parity states, associated with the $h_{11/2}$ neutron orbital, are predicted to possess triaxial shapes with $\beta_2=0.14$, $\gamma\sim-40°$, while the positive-parity states are predicted to be prolate with $\beta_2=0.16$, $\gamma\sim0°$. The large signature splitting evident for the $\nu h_{11/2}$ band 2 in ^{121}Te [i.e., the $9/2^-$ state in Fig. 3(a) lies above the $11/2^-$ state, and the $13/2^-$ state lies above the $15/2^-$ state] is consistent with the large predicted triaxial shape; for a prolate shape, a much smaller signature splitting is expected. Furthermore, the small signature splittings seen for bands 5 and 6 in Fig. 3(b) are consistent with the predicted prolate shape for the positive-parity high-Ω $\nu d_{5/2}$ and $\nu g_{7/2}$ orbitals. Finally, the larger signature splitting of band 7 is consistent with a prolate low-Ω $\nu d_{3/2}$ orbital.

At high spin, above $I=18\hbar$, well-deformed energy minima appear in the TRS calculations with deformation parameters $\beta_2\geqslant0.36$, $\gamma\sim+25°$ for both positive- and negative-parity configurations in ^{121,122}Te; these minima correspond to the rotational intruder bands. In the following sections, the low-spin noncollective oblate states are discussed in more detail. The oblate states predicted for ^{121,122}Te are summarized in Tables III and IV, while examples of these favoured states are shown in Fig. 6 as $\beta_2-\gamma$ plots.

1. Even-A Te isotopes

For even-A Te isotopes, a favored noncollective oblate state is predicted at $I^\pi=16^+$ based on the fully aligned $\pi[(g_{7/2})^2]_{6^+}\otimes\nu[(h_{11/2})^2]_{10^+}$ configuration [15]; low-lying 16^+ states have indeed been observed in ^{114}Te [4], ^{116}Te [5], ^{118}Te [6], and ^{120}Te [7], which may be identified with this oblate state. The TRS results for ^{122}Te are shown in Fig. 6(a), which show the noncollective 16^+ minimum on the oblate $\gamma=+60°$ Y-axis competing with the triaxial collective minimum at $\gamma=-43°$, based on the 2-quasineutron $\nu[(h_{11/2})^2]$ configuration. Figure 7(a) shows an experimental rigid-rotor plot for ^{122}Te, where a rotating liquid-drop energy reference, equal to $(\hbar^2/2\mathscr{J}_{\rm rig})I(I+1)$ MeV, has been subtracted. The rigid-body moment of inertia $\mathscr{J}_{\rm rig}$ has been normalized to ^{158}Er [32], such that $(\hbar^2/2\mathscr{J}_{\rm rig})=0.007(158/A)^{5/3}$ MeV, where A is the mass number. The yrast 16^+ state of Fig. 7(a) (labeled A in Fig. 1) may be identified with the fully aligned 16^+ oblate state.

A low-lying negative-parity $I^\pi=14^-$ noncollective oblate state is also predicted for the light Te isotopes with $A\leqslant120$, based on the aligned $\pi[(g_{7/2})^2]_{6^+}\otimes\nu[(d_{5/2})(h_{11/2})]_{8^-}$ configuration. Low-lying 14^- states have been observed in ^{112}Te [3], ^{114}Te [4], and ^{116}Te [5], which may be identified with this oblate state. No such states have however been observed in the heavier even-A Te isotopes, including ^{122}Te.

The TRS calculations also predict favoured oblate states at $I^\pi=22^+$ and 22^- in ^{122}Te, based on fully aligned aligned $\pi[(g_{7/2})^2]_{6^+}\otimes\nu[(h_{11/2})^4]_{16^+}$ and $\pi[(g_{7/2})^2]_{6^+}\otimes\nu[(d_{5/2})(h_{11/2})^3]_{16^-}$ configurations, respectively. However, states in ^{122}Te were not populated up to these spins in the present experiment.

2. Odd-A Te isotopes

In the case of odd-A Te isotopes, unusually low-lying $39/2^-$ states have been observed in ^{117}Te [8] and ^{119}Te [9]. The TRS calculations suggest a fully aligned $\pi[(g_{7/2})^2]_{6^+}\otimes\nu[(h_{11/2})^3]_{27/2^-}$ noncollective oblate configuration for these states. TRS results for the corresponding state in ^{121}Te are shown in Fig. 6(b), while an experimental rigid-rotor plot is shown in Fig. 7(b). The $39/2^-$ state [labeled C in Fig. 3(a)] is seen to be favored, together with the states at $I^\pi=23/2^-$ (B), and $21/2^-$ (A). These latter states are associated with noncollective oblate $\pi[(g_{7/2})^2]_{6^+}\otimes\nu[h_{11/2}]_{11/2^-,9/2^-}$ configurations, and similar states are also seen in the lighter odd-A isotopes. The TRS results for the $21/2^-$ state in ^{121}Te are shown in Fig. 6(c).

TABLE IV. TRS calculated favored noncollective oblate ($\gamma=+60°$) states in ^{121}Te.

(Parity, signature)	I^π	β_2	Aligned configuration
(−,±1/2)	$21/2^-$,$23/2^-$	0.123	$\pi[(g_{7/2})^2]_{6^+}\otimes\nu[(h_{11/2})]_{9/2^-,11/2^-}$
(−,±1/2)	$37/2^-$,$39/2^-$	0.135	$\pi[(g_{7/2})^2]_{6^+}\otimes\nu[(h_{11/2})^3]_{25/2^-,27/2^-}$
(+,±1/2)	$49/2^+$,$47/2^+$	0.135	$\pi[(g_{7/2})^2]_{6^+}\otimes\nu[(d_{5/2}/g_{7/2})^3(h_{11/2})^2]_{37/2^+,35/2^+}$

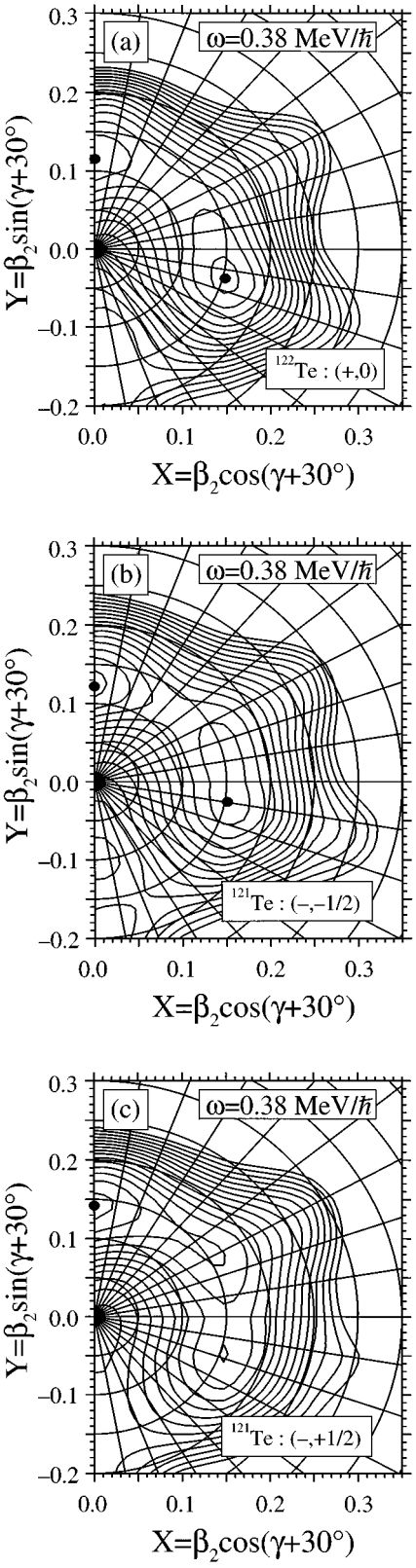

FIG. 6. Examples of TRS predicted aligned noncollective oblate states (on the y axis) at $I^{\pi}=16^{+}$ in ^{122}Te (a), $I^{\pi}=39/2^{-}$ in ^{121}Te (b), and $I^{\pi}=21/2^{-}$ in ^{121}Te (c). The energy contours are separated by 140 keV.

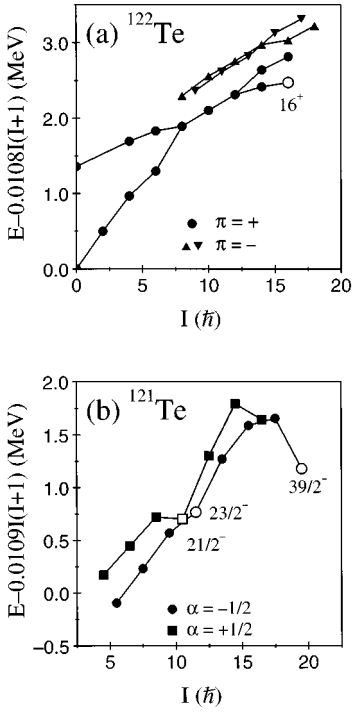

FIG. 7. Experimental rigid-rotor plots for ^{122}Te (a) and ^{121}Te (b). The open symbols represent proposed noncollective states which are labeled by spin and parity.

The oblate interpretation for the $23/2^{-}$ and $21/2^{-}$ states in band 2 is further corroborated by the extremely large $B(M1;I\rightarrow I-1)/B(E2;I\rightarrow I-2)$ ratio extracted for $I=23/2$, as shown in Fig. 5. The high value for the ratio implies a large single-particle overlap between the oblate $23/2^{-}$ and $21/2^{-}$ states, in addition to low collectivity for the 679 keV $E2$ transition.

Finally, noncollective oblate states are predicted at $I^{\pi}=47/2^{+}$ and $49/2^{+}$ in ^{121}Te, as shown in Table IV. Again, these are at a higher spin than achieved in the present experiment.

IV. CONCLUSIONS

States in ^{121,122}Te have been studied up to $I\sim 20\hbar$. The decay schemes have been discussed in terms of weakly deformed collective structures coexisting with several particularly favoured noncollective oblate states. The configurations of these states have been interpreted through comparison with TRS cranking calculations.

ACKNOWLEDGMENTS

This work was in part supported by grants from the US National Science Foundation and the UK Engineering and Physical Science Research Council. The authors are indebted to Dr. R. Wyss and Dr. W. Nazarewicz for providing the TRS cranking codes.

[1] T. Lönnroth, A. Virtanen, and J. Hattula, Phys. Scr. **34**, 682 (1986).
[2] G. Andersson, S.E. Larsson, G. Leander, P. Möller, S.G. Nilsson, I. Ragnarsson, S. Åberg, R. Bengtsson, J. Dudek, B. Nerlo-Pomorska, K. Pomorski, and Z. Szymański, Nucl. Phys. **A268**, 205 (1976).
[3] E.S. Paul, C.W. Beausang, S.A. Forbes, S.J. Gale, A.N. James, P.M. Jones, M.J. Joyce, H.R. Andrews, V.P. Janzen, D.C. Radford, D. Ward, R.M. Clark, K. Hauschild, I.M. Hibbert, R. Wadsworth, R.A. Cunningham, J. Simpson, T. Davinson, R.D. Page, P.J. Sellin, P.J. Woods, D.B. Fossan, D.R. LaFosse, H. Schnare, M.P. Waring, A. Gizon, J. Gizon, T.E. Drake, J. DeGraaf, and S. Pilotte, Phys. Rev. C **50**, 698 (1994).
[4] C.-B. Moon, J.U. Kwon, S.J. Chae, J.C. Kim, S. Bhatti, C.S. Lee, T. Komatsubara, J. Mukai, T. Hayakawa, H. Kimura, J. Lu, M. Matsuda, T. Watanabe, and K. Furuno, Phys. Rev. C **51**, 2222 (1995).
[5] A. Sharma, J. Goswamy, D. Mehta, J. Singh, H. Kaur, B. Chand, N. Singh, R.K. Bhowmik, and P.N. Trehan, Z. Phys. A **346**, 321 (1993).
[6] A. Sharma, J. Singh, H. Kaur, J. Goswamy, D. Mehta, N. Singh, R.K. Bhowmik, and P.N. Trehan, Z. Phys. A **351**, 131 (1995).
[7] P. Chowdhury, W.F. Piel, Jr., and D.B. Fossan, Phys. Rev. C **25**, 813 (1982).
[8] C. Duyar, J.E. Draper, E.C. Rubel, M.A. Deleplanque, R.M. Diamond, F.S. Stephens, E.M. Beck, and M.A. Stoyer, Z. Phys. A **348**, 63 (1994).
[9] J. Singh, H. Kaur, A. Sharma, J. Goswamy, D. Mehta, N. Singh, P.N. Trehan, E.S. Paul, and R.K. Bhowmik, Z. Phys. A **353**, 239 (1995).
[10] N. Blasi, G. Falconi, G. Lo Bianco, Ch. Protochristov, D. Bazzacco, G. De Angelis, and D.R. Napoli, Z. Phys. A **352**, 359 (1995).
[11] J. Singh, H. Kaur, A. Sharma, J. Goswamy, D. Mehta, N. Singh, R.K. Bhowmik, and P.N. Trehan, Z. Phys. A **353**, 125 (1995).
[12] W. Nazarewicz, G.A. Leander, and J. Dudek, Nucl. Phys. **A467**, 437 (1987).
[13] R. Wyss, J. Nyberg, A. Johnson, R. Bengtsson, and W. Nazarewicz, Phys. Lett. B **215**, 211 (1988).
[14] W. Nazarewicz, R. Wyss, and A. Johnson, Nucl. Phys. **A503**, 285 (1989).
[15] E.S. Paul, D.B. Fossan, J.M. Sears, and I. Thorslund, Phys. Rev. C **52**, 2984 (1995).
[16] I. Thorslund, D.B. Fossan, D.R. LaFosse, H. Schnare, K. Hauschild, I.M. Hibbert, S.M. Mullins, E.S. Paul, I. Ragnarsson, J.M. Sears, P. Vaska, and R. Wadsworth, Phys. Rev. C **52**, R2839 (1995).
[17] J.M. Sears, D.B. Fossan, D.R. LaFosse, H. Schnare, I. Thorslund, P. Vaska, K. Hauschild, I.M. Hibbert, S.M. Mullins, E.S. Paul, R. Wadsworth, A.V. Afanasjev, and I. Ragnarsson (unpublished).
[18] J.M. Sears, D.B. Fossan, D.R. LaFosse, H. Schnare, I. Thorslund, P. Vaska, K. Hauschild, I.M. Hibbert, S.M. Mullins, E.S. Paul, R. Wadsworth, A.V. Afanasjev, and I. Ragnarsson (unpublished).
[19] R. Wadsworth, H.R. Andrews, R.M. Clark, D.B. Fossan, A. Galindo-Uribarri, V.P. Janzen, J.R. Hughes, D.R. LaFosse, S.M. Mullins, E.S. Paul, D.C. Radford, P. Vaska, M.P. Waring, D. Ward, J.N. Wilson, and R. Wyss, Nucl. Phys. **A559**, 461 (1993).
[20] V.P. Janzen, D.R. LaFosse, H. Schnare, D.B. Fossan, A. Galindo-Uribarri, J.R. Hughes, S.M. Mullins, E.S. Paul, L. Persson, S. Pilotte, D.C. Radford, I. Ragnarsson, P. Vaska, J.C. Waddington, R. Wadsworth, D. Ward, J.N. Wilson, and R. Wyss, Phys. Rev. Lett. **72**, 1160 (1994).
[21] I. Ragnarsson, V.P. Janzen, D.B. Fossan, N.C. Schmeing, and R. Wadsworth, Phys. Rev. Lett. **74**, 3935 (1995).
[22] A.V. Afanasjev and I. Ragnarsson, Nucl. Phys. **A586**, 377 (1995).
[23] U. Hagemann, H.-J. Keller, Ch. Protochristow, and F. Stary, Nucl. Phys. **A329**, 157 (1979).
[24] C.S. Lee, J.A. Cizewski, D. Barker, R. Tanczyn, G. Kumbartzki, J. Szczepanski, J.W. Gan, H. Dorsett, R.G. Henry, L.P. Farris, and H. Li, Nucl. Phys. **A528**, 381 (1991).
[25] D.C. Radford, Nucl. Instrum. Methods A **361**, 297 (1995).
[26] K.S. Krane, R.M. Steffen, and R.M. Wheeler, Nucl. Data Tables **A11**, 351 (1973).
[27] K. Heyde, P. Van Isacker, R.F Casten, and J.L. Wood, Phys. Lett. **155B**, 303 (1985).
[28] Y. Liang, D.B. Fossan, J.R. Hughes, D.R. LaFosse, T. Lauritsen, R. Ma, E.S. Paul, P. Vaska, M.P. Waring, and N. Xu, Phys. Rev. C **45**, 1041 (1992).
[29] J.R. Hughes, D.B. Fossan, D.R. LaFosse, Y. Liang, P. Vaska, and M.P. Waring, Phys. Rev. C **44**, 2390 (1991).
[30] W. Nazarewicz, J. Dudek, R. Bengtsson, and I. Ragnarsson, Nucl. Phys. **A435**, 397 (1985).
[31] S. Cwiok, J. Dudek, W. Nazarewicz, W. Skalski, and T. Werner, Comp. Phys. Commun. **46**, 379 (1987).
[32] J. Simpson, M.A. Riley, S.J. Gale, J.F. Sharpey-Schafer, M.A. Bentley, A.M. Bruce, R. Chapman, R.M. Clark, S. Clarke, J. Copnell, D.M. Cullen, P. Fallon, A. Fitzpatrick, P.D. Forsyth, S.J. Freeman, P.M. Jones, M.J. Joyce, F. Liden, J.C. Lisle, A.O. Macchiavelli, A.G. Smith, J.F. Smith, J. Sweeney, D.M. Thompson, S. Warburton, J.N. Wilson, T. Bengtsson, and I. Ragnarsson, Phys. Lett. B **327**, 187 (1994).